International Journal of Computational Research and Development (IJCRD)
Impact Factor: 4.775, ISSN (Online): 2456 - 3137
(www.dvpublication.com) Volume 1, Issue 2, 2016

MULTILEVEL DAPPLE BASED CONTEXT ANALYSIS IN PULMONARY NODULE

P. John Vivek* & D. Sathya Priya, V. Sathya Priya** & T. J. Nandhini****

* Assistant Professor, Paavai Engineering College, Namakkal, Tamilnadu

** UG Students, Department of Electronics and Communication Engineering, Paavai Engineering College, Namakkal, Tamilnadu

Cite This Article: P. John Vivek & D. Sathya Priya, V. Sathya Priya & T. J. Nandhini, "Multilevel Dapple Based Context Analysis in Pulmonary Nodule", International Journal of Computational Research and Development, Volume 1, Issue 2, Page Number 6-11, 2016.

Abstract:

Lung nodule or lung lobe is a small masses of tissue in the lung as quite common. Now adays, the image processing mechanisms are used in number of medical profession for improving detection of lung cancer. The identification of the lobar fissures in CT images are very difficult even for experienced surgeons because of its variable shape and their appearance along with low contrast and high noise with it. Existing works on lung nodule were carried out just to detect the presence or absence in nodule using SVM with MR-8 classifier. In this paper presents a novel recognition method of pulmonary nodule but in this the detection of intersection and overlapping in a pulmonary nodule is performed based on the concept of multilevel dapple which partitions the image into an orderless collection of small patches. The classification is carried out using Neural network with MR-16 filters which provides a clear description of patches. This technique is a supervised learning system. In this paper also describes a three steps to extract features are; lung segmentation with adaptive fissure to segments the lobe then detection level carried out by canny edge to detect accurate location then the classifier used as MR-16.It is to reduce redundancy of image data in order to be able to store or transmit data in an efficient form. The main contribution of proposed is to find lobar fissures with accurate detection rate.

Index Terms: Classification, Feature Design, Latent Semantic Analysis & Patch Division

1. Introduction:

Lung cancer is a major cause of cancer-related deaths in humans worldwide. Approximately 20% of cases with lung nodules represent lung cancers [1]; therefore, the identification of potentially malignant lung nodules is essential for the screening and diagnosis of lung cancer [2]–[4]. Lung nodules are small masses in the human lung, and are usually spherical; however, they can be distorted by surrounding anatomical structures, such as vessels and the adjacent pleura [5]. Intra-parenchymal lung nodules are more likely to be malignant than those connected with the surrounding structures [6], and thus lung nodules are divided into different types according to their relative positions. At present, the classification from Diciotti *et al.* [7] is the most popular approach and it divides nodules into four types: well-circumscribed (W) with the nodule located centrally in the lung without any connection to vasculature; vascularized (V) with the nodule located centrally in the lung but closely connected to neighboring vessels; juxtapleural (J) with a large portion of the nodule connected to the pleural surface; and pleural-tail (P) with the nodule near the pleural surface connected by a thin tail. Sample images are shown in Fig. 1, with the nodule encircled in red. Computed tomography (CT) is the most accurate imaging modality to obtain anatomical information about lung nodules and the surrounding structures [8]–[10]. In current clinical practice, however, interpretation of CT images is challenging for radiologists due to the large number of cases. This manual reading can be error-prone and the reader may miss nodules and thus a potential cancer. Computer-aided diagnosis (CAD) systems would be helpful for radiologists by offering initial screening or second opinions to classify lung nodules [11], [12]. CADs provide depiction by automatically computing quantitative measures, and are capable of analyzing the large number of small nodules identified by CT scans.

A. Related Works: A patch-based approach, which is based on partitioning the original image into an orderless collection of smaller patches, is usually used to construct the bag-of-feature model [19]. Com-pared to an overall description of the image, patch-based methods can capture local details to better represent the heterogeneous structures. Thus, such methods can be suitable for images of lung nodules that usually contain different anatomical structures. To date, patch-based approaches have been mainly designed for some medical and general imaging problems [19]– [23] other than lung nodule classification. Patch division methods normally divide the image into square patches or into circular sector patches. The partitioning is performed in a rigid manner, i.e., the shape and size of each patch are predefined, which unavoidably groups unrelated objects together. In particular, a rigid partition on lung nodule images would mix different contextual structures in one patch and cause difficulty in context description. Ideally, one patch should depict a single type of anatomical structure, and the formulation of patches should be adaptive to the local information. Super pixel formulation [24]–[26] pro-vides an efficient tool for this aim, within each patch the pixels are closely related (*e.g.*, similar intensities). Although quick shift shows its advantages on handling lung nodule image by incorporating the local spatial information and reducing spurious labeling due to noise, direct use of quick shift on such small images would group heterogeneous contents together. Therefore, the original quick shift process needs improvement to

obtain better patches.

B. Outline of the Proposed Method: In light of the above, this paper presents a novel image classification method for the four common types of lung nodules. We suggest that the major contributions of our work are as follows: i) a patch-based image representation with multilevel concentric partition, ii) a feature set design for image patch description, and iii) a contextual latent semantic analysis-based classifier to calculate the probabilistic estimations for each lung nodule image. More specifically, a concentric level partition of the image is designed in an adaptive manner with: (1) an improved super pixel clustering method based on quick shift is designed to generate the patch division; (2) multilevel partition of the derived patches is used to construct level-nodule (i.e., patches containing the nodules), and level-context (i.e., patches containing the contextual structures). A concentric level partition is thus constructed to tackle the rigid partitioning problem. Second, a feature set of three components is extracted for each patch of the image that are as follows:

- ✓ a SIFT descriptor, depicting the overall intensity, texture, and gradient information;
- ✓ a MR8+LBP descriptor, representing a richer texture feature incorporating MR8 filters before calculating LBP histograms;
- ✓ a multiorientation HOG descriptor, describing the gradients and accommodating rotation variance in a multicoordinate system.

Third, the category of the lung nodule image is finally deter-mined with a probabilistic estimation based on the combination of the nodule structure and surrounding anatomical context: (1) SVM is used to compute the classification probability based on level-nodule; (2) pLSA with contextual voting is employed to calculate the classification probability based on level-context. The designed classifier can obtain better classification accuracy, with SVM capturing the differences from various nodules, and pLSA further revising the decision by analyzing the context. The structure of this paper is as follows. Sections II, III, and IV describe the three stages of the proposed method concentric level construction, feature extraction, and context analysis classification. Section V introduces the experiment dataset and the outline of the experiment design, and Section VI presents the experimental results and discussions. Finally, the conclusion and future work are given in Section VII.

2. Feature Extraction:

The effectiveness of image feature description depends on: distinction and invariance [16], which means that the descriptor needs to capture the distinctive characteristics and be robust to adapt to the various imaging conditions. Based on our visual analysis the lung nodules, we suggest that intensity, texture, and gradient can characterize the various nodules and the diverse contextual structures. We thus designed the feature set of the combination of SIFT for overall description, MR8+LBP for texture, and multiorientation HOG for gradient. For convenience, we refer to this feature set as the FS3 feature.

A. SIFT Descriptor for Overall Description: The SIFT process generates a 128-length vector for each key point. Since SIFT is invariant to image translation, scaling, rotation and illumination changes, and robust to local geometric distortion, it provides valuable lung nodule data [4], [16], [17]. SIFT is robust and is able to carry out semantic classification due to its ability to capture the texture and gradient information [47], [48]. Besides, it identifies the key points by computing extremum pixels in the image local area to incorporate the intensity information. Thus, $SIFT^2$ descriptor was adopted as the first component of FS3 to give an overall description from intensity, texture, and gradient perspectives.

B. MR8+LBP Descriptor for Texture Description: The combination of MR8 filters and LBP feature is designed to provide richer texture description of patches by incorporating multiscale and rotation-invariant properties. LBP is a powerful feature for texture based image classification [35], [49]. Although LBP can be easily configured to describe the local texture structure with multiresolution and rotation-invariance, it captures too many trivial image variations. Therefore, we in-corporate the MR filter set before computing LBP histogram. The MR set contains both isotropic and anisotropic filters at multiple orientations and multiple scales and records the angle of maximum response, which makes it possible to discriminate textures that appear to be very similar. Specifically, MR8 bank [50] is used in our method, which consists of 38 filters but produces only eight filter responses by recording only the maximum filter response across all orientations for one scale. This yields rotation invariance. The final filter response contains two anisotropic filters for each of three different scales and two isotropic filters ($2 \times 3 + 2$). MR8 filters are directly applied to the original image, as shown in Fig. 5. For image I, we get eight filter responses represented by $I_{\mathrm{MR8}}(f)$ where $f \in [1, 8]$.

C. Multiorientation HOG Descriptor for Gradient: Gradient distribution provides helpful supplementary in-formation to texture for discriminating various anatomical structures in nodule images. Among various gradient-based methods, HOG is being widely used and can also improve performance considerably when coupled with LBP [27]. However, unlike SIFT and MR8+LBP descriptors, the raw HOG descriptor cannot handle rotation-invariant problems. Therefore, we designed a multiorientation HOG descriptor inspired by our previous work [51] to provide further an advanced gradient description in addition to that from SIFT. The designed descriptor is adaptive to the locations of patches relative to the centroid of the nodule, rather than having the same initial orientation for all patches [51]. Assuming that the center of patch pa_o is $c_{pa\ o}$, we built eight coordinate systems that share the same origin $c_{pa\ o}$ but have different initial orientations (0 degree). A visual illustration of the

multicoordinate systems is shown in Fig. 6(c). Two of them are shown with (x0, y0) and (x1, y1). Contra-rotating the first coordinate system (i.e., (x0, y0)) by 45 degree generates the next one (i.e., (x1, y1)). Instead of predefining the initial orientation of the first coordinate system, we set it as the direction (blue dash line) from the centroid of the patch (green area) to the centroid of lung nodule (yellow area).

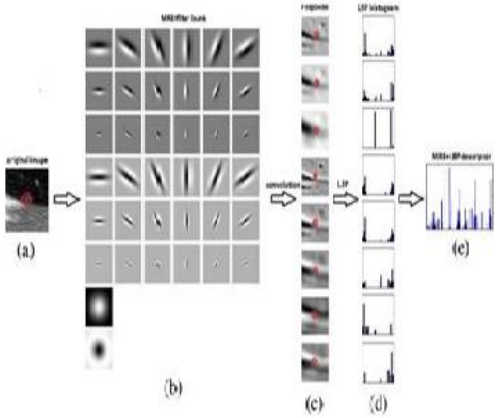

Figure 1 Illustration of the generation of the MR8+LBP descriptor: (a) the original image with the target patch pa_o with a red circle, (b) 38 filters with six orientations at three scales for two oriented filters, and two isotropic filters ($6 \times 3 \times 2 + 2$), (c) eight image filter responses with three scales for two filters and two isotropic filters ($3 \times 2 + 2$), (d) histograms of the select patch pa_o in the eight responses by computing the LBP descriptor, (e) the final MR8+LBP descriptor produced by concatenating all histograms. Next, for each coordinate system, patch pa_o is divided into nine cells, within which gradient orientations of the pixels in nine undirected histograms are counted to encode the gradient distribution. Instead of adopting the histogram statistics directly, we apply the *UOCTTI* variant from Felsenszwalb *et al.* [52] which computes the *L1* norm of each of the *L2* normalized undirected histograms to get a four-dimensional (4-D) texture-energy feature for each coordinate system, as shown in Fig. 6(d). As a result, for patch pa_o , we obtain a 288-length (eight systems × nine cells × 4-D features) multiorientation HOG descriptor MHOG(pa_o), as shown in Fig2.

3. Context Analysis Classification:

With the concentric level partition and feature set, the next stage is to label each image with one of the four nodule categories. Considering that the morphology of lung nodules forms a continuum [17], which means the structures of lung nodules among different categories are similar, even with the comprehensive feature design, it remains difficult to classify the images precisely. So to aid classification, we incorporated the contextual information. The proposed method involves SVM analysis for lung nodule patches, and pLSA analysis for context patches. In a supervised manner, besides the explicit label information (with SVM), we also extracted the implicit latent semantic information hidden in the relationship between the images and their categories (with pLSA). In this way, the training data are used twofold, which acquires much more information. The first step is lung nodule probability estimation using SVM. This step works on level-nodule that focuses on lung nodule description. The proposed feature sets are extracted for all patches in level-0, and the SVM classification procedure is performed with a probability estimate [17]. For each lung nodule image I , we thus compute its probability of each of the four types $TP = \{tp_t \mid t \in \{w, v, j, p\}\}$ based on level-nodule, called the level-nodule probability.

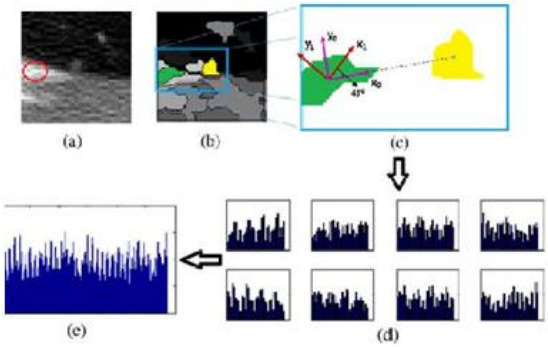

4. Experimental Results and Discussions:

Finally, the effect of weight parameter λ on the classification results is shown in Fig. 9. Although the classification rates on the training dataset tend to be a little higher than that on the testing dataset when λ is smaller (from 0 to 0.5), they are similar when λ is relatively larger (from 0.6 to 1). The similar classification rate distributions for the training and testing datasets suggest the balanced performance of the proposed method on

both the labeled and unlabeled images. In addition, it can be observed that combining both level-nodule probability and level-context probability resulted in better performance than using the individual contribution separately. Specifically, the best results were achieved when $\lambda = 0.7$, indicating level-nodule contributes more to the final decision. Therefore, λ was fixed at 0.7.

5. Experimental Results and Discussions:

Finally, the effect of weight parameter λ on the classification results is shown in Fig. 9. Although the classification rates on the training dataset tend to be a little higher than that on the testing dataset when λ is smaller (from 0 to 0.5), they are similar when λ is relatively larger (from 0.6 to 1). The similar classification rate distributions for the training and testing datasets suggest the balanced performance of the proposed method on both the labeled and unlabeled images. In addition, it can be observed that combining both level-nodule probability and level-context probability resulted in better performance than using the individual contribution separately. Specifically, the best results were achieved when $\lambda = 0.7$, indicating level-nodule contributes more to the final decision. Therefore, λ was fixed at 0.7.

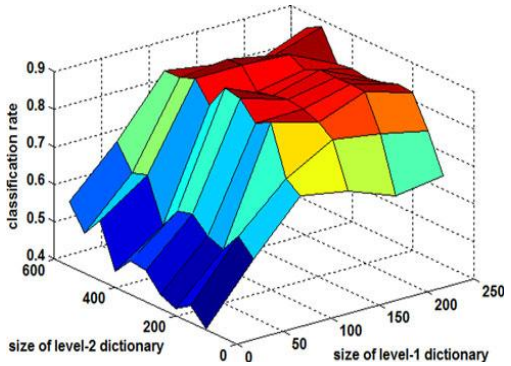

Figure 4: Distribution of classification rates given sizes of the two dictionaries: the rate tends to be stable after *N*level-1 is 100 and *N*level-2 is 200, shown in the red area.

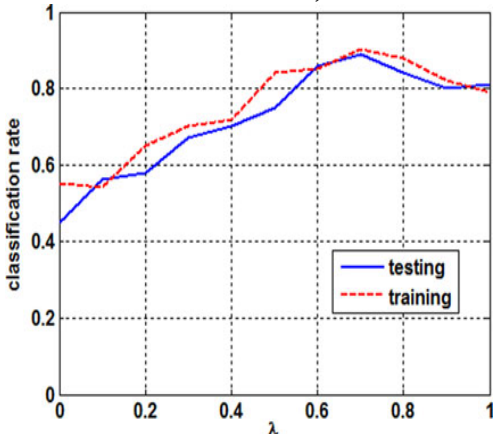

Figure 5: Distributions of classification rates given parameter λ on the training and testing datasets

B. Evaluation of Concentric Level Partition: To illustrate the effect of the proposed concentric level partition, we present the quantitative comparisons among the following methods: the rigid partition, quick shift on the original image, quick-shift based on amplification and down sampling without iterative formulation, and our method. Except for the second approach that extracted too few patches to construct the multilevel partition structure, the other two were handled in the following manner to construct a two-level partition structure as for the proposed method: (1) For the first one, 3 × 3 pix-els were regarded as one patch. The center patch was used as level-nodule, and the remaining patches were equally divided into level-1 and level-2 to build level-context; (2) For the third one, a four-level partition structure was formed. The first two context levels and the last two context levels were then combined to derive a two-level partition. For the second method, we built a one-level partition, which means the level type probability from level-1 was directly used as level-context probability. The rigid partition generated a lower rate than the last two, which proves that concentric level partition based on adaptive patch extraction can obtain better description of the image con-textual information, and further improve the classification result. The second approach obtained the lowest classification rate at about 55%, suggesting that the amplification and iterative process can improve classification performance. Also, while the last two had quite similar results, our iterative scheme outperformed the other ones, with a shorter running time due to a smaller number of extracted patches (the third method generated more than five times as many patches as those from the proposed method). Except for the advantage of the improved quick shift process, the comparison with the second approach that uses level type probability to directly predict level-context probability also shows the necessity of the contextual voting, as we discussed in Section IV that it is undesirable to estimate the type of

lung nodule image directly based on level types because similar contexts could be shared among different types of lung nodules.

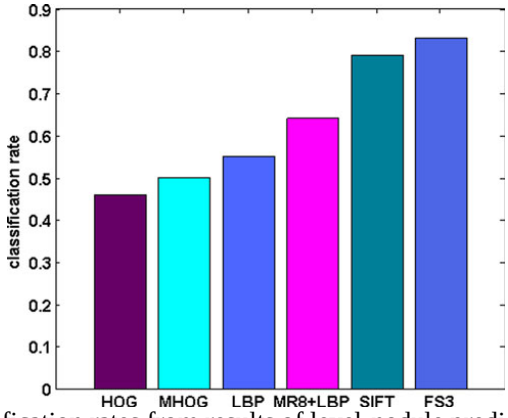

Figure 6: Comparison of classification rates from results of level-nodule prediction based on different feature descriptors: (1) original HOG; (2) multiorientation HOG; (3) original LBP; (4) MR8+LBP; (5) SIFT, and (6) FS3.

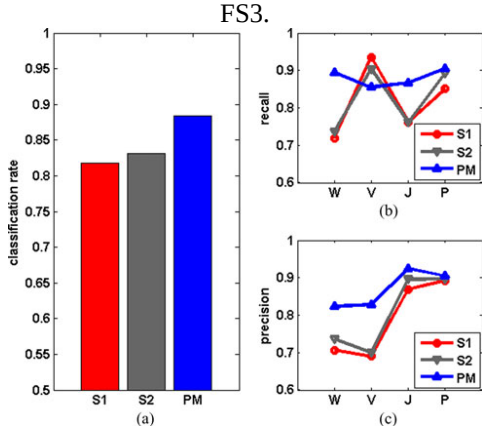

Figure 7: Comparison between SVM and the proposed classifier: (a) classification rate, (b) recall, (c) precision

C. Evaluation of Feature Extraction: The designed FS3 feature describes the image content from different aspects, i.e., intensity, texture, and gradient, with the three component descriptors. To measure if the combination of them provides an advanced description of the image, we com-pared it with those three components individually. Also, the original LBP and HOG were tested to show the advantages of the designed MR8+LBP and multiorientation HOG descriptors. Here, instead of using the proposed classifier, we simply classified the images according to level-nodule probability, which was computed from the nodule patch with SVM. In this way, we hoped to eliminate the influence from the context analysis, and merely focus on feature design comparison. The comparison results are shown in Fig. 11. Raw HOG generated the worst result among all approaches, since it works on uniformly spaced cells instead of focusing on particular points, and thus it is deficient for acquiring the most distinctive characterization among the various patches. The de-signed multiorientation HOG descriptor outperformed the raw HOG descriptor, indicating the benefit of handling the rotation-invariant problem for feature description. However, multiorientation HOG achieved a result with only close to 50% of images accurately classified, suggesting that simply accommodating the rotation problem is still not sufficient to capture the spherical shape of lung nodules. MR8+LBP descriptor achieved about a 5% improvement on classification rate compared with raw LBP, suggesting the benefit of MR8 filters in discriminating the similar textures through its multiorientation and multiscale properties and its ability to eliminate some unnecessary imaging details. The better performances of LBP-based approaches over the HOG-based approaches indicate that lung nodule structure can be better characterized by textures other than gradients; however, its lower classification rate compared with SIFT suggests integrating the intensities, textures, and gradient can provide a better feature descriptor.

D. Evaluation of Classifier: The proposed classifier categorizes the lung image based on the concentric level partition and the extracted feature. The level-nodule probability and level-context probability are combined to classify the images. To evaluate our design of the classifier, comparisons were conducted across our proposed method (PM), the SVM on level-nodule (S1), and the SVM with con-text analysis (S2) on the overall classification rate and also to measure the recall and precision for each individual type. The second approach is the calculation of level-nodule probability. The third approach contains level-nodule probability and level-context probability; however, the level-context only contains a single level which is composed of all context patches, and a SVM model is trained, based on the distribution of topics calculated with pLSA to compute the

level-context probability. The dictionary size N , topic size K, and weighed parameter λ for this approach were settled as 350, 350, and 0.6, which obtained the highest classification rate. Fig. 12 illustrates the comparison results. The classification rates of the two SVM-based approaches were quite similar at about 82% and 83%. The relatively small enhancement with S2 shows the benefit of context analysis, and also indicates the limit of SVM with its direct classification manner for lung nodule context identification. About 7% more of the images were correctly classified using the proposed classifier (89%) than only adopting level-nodule probability (S1, 82%), suggesting that integrating the level-context probability with level-probability is helpful for lung nodule image classification. Also, about 6% improvement was obtained over S2, indicating that the designed context analysis scheme based on multilevel partition and contextual voting is more suitable for lung nodule context analysis. This enhancement strongly depends on level-type identification and contextual voting. Taking the type W and V as examples, although images from both of them contain a similar level type sequence V-J, the credit of V-J on image type W is 0.36 that is twice as the credit on image type V, showing more images with sequence V-J belong to type W. Therefore, with the help of the voting process, more images in type W were correctly classified, as well as type J. Meanwhile, images that are not clearly distinguished between these three categories would also be more likely to be classified into type W and J, thus more of the actual type V were misclassified than the two control methods, leading to a relatively lower recall of type V. Ultimately, although the misclassification rate of type V to other types was increased in the proposed method, those of the other types were decreased to a larger extent, leading to the more balanced distributions of recall and precision and a better overall classification rate.

6. Conclusion:

We present a supervised classification method for lung nodule LDCT images in this paper. The four main categories of lung nodules well-circumscribed, vascularized, juxta-pleural, and pleural-tail were the objects to be differentiated. We de-signed a novel method to overcome the problem of the lung nodule overlapping adjacent structures. Our method had three components: concentric level partition, feature extraction, and context analysis classification. A concentric level partition was constructed by an improved quick shift super pixel formulation. Then, a FS3 feature set including SIFT, MR8+LBP, and multiorientation HOG was generated to describe the image patch from various perspectives. Finally, a supervised classifier was designed through combining level-nodule probability and level-context probability. The results from the experiments on the ELCAP dataset showed promising performance of our method. We also suggest that the proposed method can be generally applicable to other medical or general imaging domains. For instance, the improved quick shift formulation process could be applied as the preprocessing stage for patch-based imaging anal-ysis; the extracted feature set could be employed as a feature descriptor for other kinds of images; and the latent semantic analysis with the voting process could be used for analyzing hierarchical image patches.

7. References:

1. J. J. Erasmus, J. E. Connolly, H. P. McAdams, and V. L. Roggli, “Solitary pulmonary nodules: Part I. morphologic evaluation for differentiation of benign and malignant lesions,” Radiographics, vol. 20, no. 1, pp. 43–58, 2000.
2. D. Wu, L. Lu, J. Bi, Y. Shinagawa, K. Boyer, A. Krishnan, and M. Salganicoff, “Stratified learning of local anatomical context for lung nodules in CT images,” in Proc. Comput. Vis. Pattern Recog., 2010, pp. 2791–2798.
3. Roback, M. F. McNitt-Gray, and M. S. Brown, “Automated classification of lung bronchovascular anatomy in CT using adaboost,” Med. Image Anal., vol. 11, no. 3, pp. 315–324, 2007.
4. A. Farag, S. Elhabian, J. Graham, A. Farag, and R. Falk, “Toward precise pulmonary nodule descriptors for nodule type classification,” in Proc. Med. Image Comput. Comput.-Assisted Intervention Conf. Lecture Notes Comput. Sci., 2010, vol. 13, no. 3, pp. 626–633.
5. A. Farag, “A variational approach for small-size lung nodule segmentation,” in Proc. Int. Symp. Biomed. Imag., 2013, pp. 81–84.
6. D. Xu, H. J. van der Zaag-Loonen, M. Oudkerk, Y. Wang, R. Vliegenthart, E. T. Scholten, J. Verschakelen, M. Prokop, H. J. de Koning, and R. J. van Klaveren, “Smooth or attached solid indeterminate nodules detected at baseline CT screening in the NELSON study: Cancer risk during 1 year of follow-up,” Radiology, vol. 250, no. 1, pp. 264–272, 2009.